The Influence of Surface Deformations on Electroencephalographic Recordings

George Dassios, Michael Doschoris and George Fragoyannis

***Abstract*— The precise identification of neuronal currents via Electroencephalographic (EEG) recordings is an important aspect in clinical practice and strongly depends on the accuracy of the corresponding forward problem. In addition, the precision of the EEG forward model is closely connected to the existence of a volume conductor model as realistic as possible. In this paper, the impact of geometric variations of the head on the measured electric potential has been studied by means of a homogeneous spherical conductor. In the case where the activated region is situated in the vicinity of the deformation, the calculated potential values show a slight increase. On the other hand, for neuronal currents away from the deformation no influence upon the surface electric measurements is observed.**

I. INTRODUCTION

Reconstruction of cerebral activity via Electroencephalographic (EEG) and Magnetoencephalographic (MEG) recordings are established tools in clinical diagnosis and cognitive research. A requirement in order to investigate the brains electromagnetic activity is the existence of a realistic volume conductor model. Typically, the head-brain system is modeled either as a simple homogeneous sphere or by a set of spherical shells with varying conductivities, producing closed form solutions which, as a consequence, provide insight to the observed phenomena.

However, computer model simulations [1], [2], [3] suggest that neglecting geometric variations present at the conductors surface (such as skull thickness, cavities, etc.) strongly influence the forward EEG problem and therefore the accuracy of the reconstruction process for the source.

Nonetheless, in order to understand the problem a rigorous mathematical analysis is needed. The present study consist a first approach towards this direction. Employing a homogeneous spherical conductor the effect of surface deformations on the forward EEG problem is analyzed.

The article is organized as follows. The first part of Section 2 provides the necessary mathematical background for the forward EEG problem. In the second part, employing standard perturbation techniques, the first order perturbation of the corresponding Poincaré expansion is explicitly calculated. Finally, section 3 provides numerical examples.

G. Dassios[1] and M. Doschoris[2] are with the Division of Applied Mathematics, Department of Chemical Engineering, University of Patras, as well as with the Institute of Chemical Engineering Sciences, FORTH/ICE-HT, GR 26504 Rio, Hellas. [1]dassios@iceht.forth.gr
[2]mdoscho@chemeng.upatras.gr

G. Fragoyannis is with the Department of Computer Engineering & Informatics, University of Patras, GR 26504 Rio, Hellas. gfrago@upatras.gr

II. THE FORWARD EEG PROBLEM.

Activation of a localized region in the brain triggers a primary neuronal current $\mathbf{J}^{\mathrm{p}}(\mathbf{r})$ leading to a measurable electric potential on the surface of the head.

In the case where the neuronal current is represented by a single equivalent dipole at the point $\mathbf{r}_0$ with moment $\mathbf{Q}$, then $\mathbf{J}^{\mathrm{p}}(\mathbf{r}) = \mathbf{Q}\,\delta(\mathbf{r}-\mathbf{r}_0)$, δ denoting the Dirac measure.

Approximating the head-brain system by a spherical homogeneous conductor with radius a and conductivity σ, the *interior* electric potential $u^-(\mathbf{r})$ solves the following problem

$$\Delta\, u^-(\mathbf{r}) = \frac{1}{\sigma}\mathbf{Q}\cdot\nabla\delta(\mathbf{r}-\mathbf{r}_0), \quad r<a, \tag{1}$$

$$\frac{\partial}{\partial r}\, u^-(\mathbf{r}) = 0, \quad r=a, \tag{2}$$

where the operators Δ and ∇ act on the point of observation $\mathbf{r}$.

Once the above problem is solved, knowledge of the solution $u^-(\mathbf{r})$ leads to the *exterior* electric potential $u^+(\mathbf{r})$ satisfying the Dirichlet problem

$$\Delta\, u^+(\mathbf{r}) = 0, \quad r>a, \tag{3}$$

$$u^+(\mathbf{r}) = u^-(\mathbf{r}), \quad r=a, \tag{4}$$

$$u^+(\mathbf{r}) = \mathcal{O}\left(\frac{1}{r^2}\right), \quad \mathbf{r}\to\infty. \tag{5}$$

Introducing an auxiliary function $\upsilon(\mathbf{r})$ as

$$u(\mathbf{r}) = \frac{1}{\sigma}\mathbf{Q}\cdot\nabla_{\mathbf{r}_0}\,\upsilon(\mathbf{r}) \tag{6}$$

and by the fact that $\nabla_{\mathbf{r}}\delta(\mathbf{r}-\mathbf{r}_0) = -\nabla_{\mathbf{r}_0}\delta(\mathbf{r}-\mathbf{r}_0)$, above BVP's simplify as follows

$$\Delta\,\upsilon^-(\mathbf{r}) = -\delta(\mathbf{r}-\mathbf{r}_0), \quad r<a, \tag{7}$$

$$\frac{\partial}{\partial r}\,\upsilon^-(\mathbf{r}) = 0, \quad r=a \tag{8}$$

as well as

$$\Delta\,\upsilon^+(\mathbf{r}) = 0, \quad r>a, \tag{9}$$

$$\upsilon^+(\mathbf{r}) = \upsilon^-(\mathbf{r}), \quad r=a, \tag{10}$$

$$\upsilon^+(\mathbf{r}) = \mathcal{O}\left(\frac{1}{r^2}\right), \quad \mathbf{r}\to\infty. \tag{11}$$

The solution regarding (7) and (8) is obtained by a straightforward expansion in spherical harmonics, i.e.

$$\upsilon^-(\mathbf{r}) = \frac{1}{4\pi}\sum_{n=1}^{\infty}\left(\frac{1}{r^{n+1}} + \frac{n+1}{n}\,\frac{r^n}{a^{2n+1}}\right) r_0^n\,\mathrm{P}_n(\hat{\mathbf{r}}\cdot\hat{\mathbf{r}}_0). \tag{12}$$

978-1-4799-3163-7/13/$31.00 ©2013 IEEE

It is possible to express above relation in closed form (see [4] for details) as

$$\upsilon^-(\mathbf{r}) = \frac{1}{4\pi}\left(\frac{1}{P} + \frac{a}{r}\frac{1}{R} - \frac{1}{a}\ln\frac{rR + \mathbf{r}\cdot\mathbf{R}}{2a^2}\right) \tag{13}$$

where

$$\mathbf{P} = \mathbf{r} - \mathbf{r}_0, \quad \mathbf{R} = \frac{a^2}{r^2}\mathbf{r} - \mathbf{r}_0. \tag{14}$$

On the other hand, the corresponding boundary values are easily evaluated to be

$$\upsilon(a\hat{\mathbf{r}}) = \sum_{n=1}^{\infty}\sum_{m=-n}^{n}\frac{1}{n}\frac{r_0^n}{a^{n+1}}\bar{\mathrm{Y}}_n^m(\hat{\mathbf{r}}_0)\mathrm{Y}_n^m(\hat{\mathbf{r}}) \tag{15}$$

$$= \frac{1}{4\pi}\left(\frac{2}{|a\hat{\mathbf{r}} - \mathbf{r}_0|} - \frac{1}{a}\ln\frac{|a\hat{\mathbf{r}} - \mathbf{r}_0| + \hat{\mathbf{r}}\cdot(a\hat{\mathbf{r}} - \mathbf{r}_0)}{2a}\right). \tag{16}$$

where an overline denotes complex conjugation and the addition formula

$$\mathrm{P}_n(\hat{\mathbf{r}}\cdot\hat{\mathbf{r}}_0) = \frac{4\pi}{2n+1}\sum_{m=-n}^{n}\bar{\mathrm{Y}}_n^m(\hat{\mathbf{r}}_0)\mathrm{Y}_n^m(\hat{\mathbf{r}}) \tag{17}$$

has been taken into account as well.

A. Effect of a Perturbed Surface on the Forward EEG Problem

Assume in the sequel a perturbed homogeneous spherical conductor, depicted in Fig. 1, each point belonging to the boundary given by the relation

$$r(\theta,\phi;\epsilon) = a + \epsilon\, f(\theta,\phi) \tag{18}$$

where ϵ is the so-called perturbation parameter and $f(\theta,\phi)$ is a smooth enough function.

Apparently, if $\epsilon = 0$, the unperturbed case described earlier is recovered. And since the unperturbed case corresponds to $\epsilon = 0$, we seek a solution in the linear regime of the form

$$\upsilon^-(\mathbf{r};\epsilon) = \upsilon_0^-(\mathbf{r}) + \epsilon\,\upsilon_1^-(\mathbf{r}) + \cdots. \tag{19}$$

The Neumann condition $\hat{\mathbf{n}}\cdot\nabla\upsilon(\mathbf{r}) = 0$, where $\hat{\mathbf{n}}$ is the unit normal on the perturbed boundary, becomes

$$r^2\frac{\partial\upsilon^-}{\partial r} - \frac{\partial r}{\partial\theta}\frac{\partial\upsilon^-}{\partial\theta} - \frac{1}{\sin^2\theta}\frac{\partial r}{\partial\phi}\frac{\partial\upsilon^-}{\partial\phi} = 0 \tag{20}$$

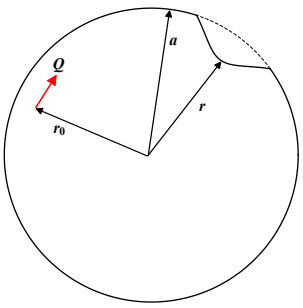

Fig. 1. A locally deformed homogeneous sphere of radius $r(\theta,\phi;\epsilon)$. The declination or elevation of the geometrical perturbation depends upon the parameter ϵ. For non-deformed regions $\epsilon = 0$ and $r(\theta,\phi;0) = a$. The dipole sources are always located inside the *perturbed* conductor.

which in view of (18), (19) and collecting coefficients supplies the necessary boundary value problem for the first correction $\upsilon_1^-(\mathbf{r})$, as

$$\Delta\,\upsilon_1^-(\mathbf{r}) = 0, \quad r < a, \tag{21}$$

$$\frac{\partial\upsilon_1^-}{\partial r} = \frac{1}{a^2}\left(\frac{\partial f}{\partial\theta}\frac{\partial\upsilon_0^-}{\partial\theta} + \frac{1}{\sin^2\theta}\frac{\partial f}{\partial\phi}\frac{\partial\upsilon_0^-}{\partial\phi}\right), \quad r = a \tag{22}$$

where υ_0^- is given by (15).

Expanding $\upsilon_1^-(\mathbf{r})$ in terms of spherical harmonics and with the aid of (15) the boundary condition reads

$$\sum_{p=1}^{\infty}\sum_{q=-p}^{p} p\,\mathcal{B}_p^q\,a^{p+1}\,r_0^p\,\hat{\mathrm{Y}}_p^q(\bar{\mathbf{r}}_0)\,\mathrm{Y}_p^q(\hat{\mathbf{r}}) = \frac{1}{\sin\theta}\frac{\partial f}{\partial\theta}$$
$$\times\sum_{n=1}^{\infty}\sum_{m=-n}^{n}\frac{r_0^n\,\bar{\mathrm{Y}}_n^m(\hat{\mathbf{r}}_0)}{na^{n+1}}\left[(2n+1)j_{n+1,m}\,\mathrm{Y}_{n+1}^m(\hat{\mathbf{r}}) - \mathrm{Y}_n^m(\hat{\mathbf{r}})\right]$$
$$+ i\frac{1}{\sin^2\theta}\frac{\partial f}{\partial\phi}\sum_{n=1}^{\infty}\sum_{m=-n}^{n}\frac{m}{n}\frac{r_0^n\,\bar{\mathrm{Y}}_n^m(\hat{\mathbf{r}}_0)}{a^{n+1}}\mathrm{Y}_n^m(\hat{\mathbf{r}}), \tag{23}$$

provided that

$$\sin\theta\,\frac{\partial}{\partial\theta}\mathrm{Y}_n^m(\hat{\mathbf{r}}) = (2n+1)j_{n+1,m}\,\mathrm{Y}_{n+1}^m(\hat{\mathbf{r}}) - \mathrm{Y}_n^m(\hat{\mathbf{r}}) \tag{24}$$

where

$$j_{n,m} = \sqrt{\frac{n^2 - m^2}{4n^2 - 1}} \tag{25}$$

and

$$\frac{\partial}{\partial\phi}\mathrm{Y}_n^m(\hat{\mathbf{r}}) = im\,\mathrm{Y}_n^m(\hat{\mathbf{r}}). \tag{26}$$

In what follows, replace

$$\frac{1}{\sin\theta}\frac{\partial f}{\partial\theta}, \quad \frac{1}{\sin^2\theta}\frac{\partial f}{\partial\phi}$$

by an expansion in terms of spherical harmonics and compute the emerging products of double series. Utilizing orthogonality the coefficients $\mathcal{B}_p^q$ are given as

$$\mathcal{B}_p^q = \frac{(-1)^q}{2pa}\sqrt{\frac{2p+1}{\pi}}\left\{\sum_{n=1}^{\infty}\sum_{k=1}^{n}\sum_{m=-k}^{k}\sum_{\ell=-n+k-1}^{n-k+1}\frac{r_0^k\,\bar{\mathrm{Y}}_k^m(\hat{\mathbf{r}}_0)}{ka^{k+1}}\right.$$
$$\times\sqrt{((k+1)^2 - m^2)(2k+1)(2n-2k+3)}\,\beta_{n-k+1}^{\ell}$$
$$\times\begin{pmatrix} k+1 & n-k+1 & p \\ 0 & 0 & 0\end{pmatrix}\begin{pmatrix} k+1 & n-k+1 & p \\ m & \ell & -q\end{pmatrix}$$
$$-\sum_{n=1}^{\infty}\sum_{k=1}^{n}\sum_{m=-k}^{k}\sum_{\ell=-n+k-1}^{n-k+1}\frac{r_0^k\,\bar{\mathrm{Y}}_k^m(\hat{\mathbf{r}}_0)}{ka^{k+1}}$$
$$\times\sqrt{(2k+1)(2n-2k+3)}(\beta_{n-k+1}^{\ell} - im\gamma_{n-k+1}^{\ell})$$
$$\left.\times\begin{pmatrix} k & n-k+1 & p \\ 0 & 0 & 0\end{pmatrix}\begin{pmatrix} k & n-k+1 & p \\ m & \ell & -q\end{pmatrix}\right\} \tag{27}$$

where

$$\beta_{n-k+1}^{\ell} = \int_0^{2\pi}\int_0^{\pi}\frac{\partial f}{\partial\theta}\bar{\mathrm{Y}}_{n-k+1}^{\ell}(\hat{\mathbf{r}})\mathrm{d}\theta\mathrm{d}\phi, \tag{28}$$

$$\gamma_{n-k+1}^{\ell} = \int_0^{2\pi}\int_0^{\pi}\frac{1}{\sin\theta}\frac{\partial f}{\partial\phi}\bar{\mathrm{Y}}_{n-k+1}^{\ell}(\hat{\mathbf{r}})\mathrm{d}\theta\mathrm{d}\phi. \tag{29}$$

The quantity

$$\begin{pmatrix} j_1 & j_2 & j_3 \\ m_1 & m_2 & m_3 \end{pmatrix}$$

is the so-called $3j$ symbol [5] satisfying the triangle condition as well as $m_1 + m_2 + m_3 = 0$.

The electric potential on the perturbed surface is then

$$\upsilon(a\hat{\mathbf{r}};\epsilon) \cong \upsilon_0(a\hat{\mathbf{r}}) + \epsilon\,\upsilon_1(a\hat{\mathbf{r}}) \tag{30}$$

where $\upsilon_0(a\hat{\mathbf{r}})$ is given by (16), whereas

$$\upsilon_1(a\hat{\mathbf{r}}) = \sum_{p=1}^{\infty}\sum_{q=-p}^{p} \mathcal{B}_p^q\, \mathrm{Y}_p^q(\hat{\mathbf{r}}) \tag{31}$$

with $\mathcal{B}_p^q$ given by (27).

III. RESULTS

The spherical head model consist of four compartments, namely: (a) The facial region (indicated with purple color in Fig. 2 and 4) located between $\theta \in [\frac{3\pi}{8}, \pi]$ and $\phi \in [\frac{3\pi}{2}, \frac{\pi}{2}]$, (b) the back of the head located between $\theta \in [\frac{3\pi}{8}, \pi]$ and $\phi \in [\frac{\pi}{2}, \frac{3\pi}{2}]$, (c) the top of the head located between $\theta \in [0, \frac{3\pi}{8}]$ and $\phi \in [0, 2\pi]$ as well as, (d) the perturbed surfaces (indicated with orange color in Fig. 2 and Fig. 4) which are reconstructed by means of the function

$$f(\theta,\phi) = (\sin k\theta)^n\,(\cos \ell\theta)^m\,. \tag{32}$$

A. Local surface distortions

For the first example, we consider a closed head injury in form of a blow to the head right above the facial region, depicted in Fig. 2, represented by (32) with parameters $(k,\ell,n,m) = (8,3,2,3)$ defined in the intervals $\theta \in [\frac{\pi}{4}, \frac{3\pi}{8}]$ and $\phi \in [\frac{3\pi}{2}, \frac{11\pi}{6}]$. The maximum depth of the deformed area, stationed central, is considered small corresponding to $\epsilon = 6 \times 10^{-3}$ m. We note, that these kind of injuries are commonly associated with home and occupational accidents as well as motor vehicle traffic collisions.

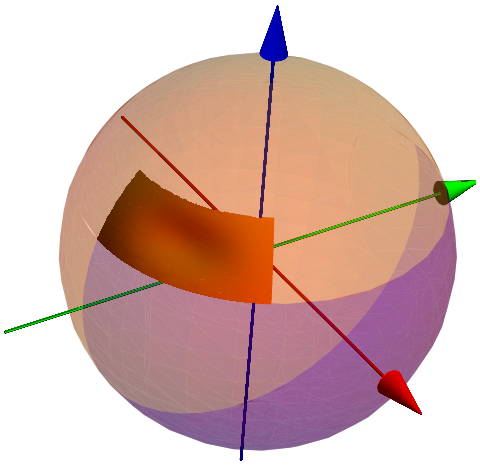

Fig. 2. A non-penetrating head injury in form of a sunken area (orange) situated at the fore part of the head, just above the facial region (purple). The red, green and blue arrows represent the x, y and z axis, respectively.

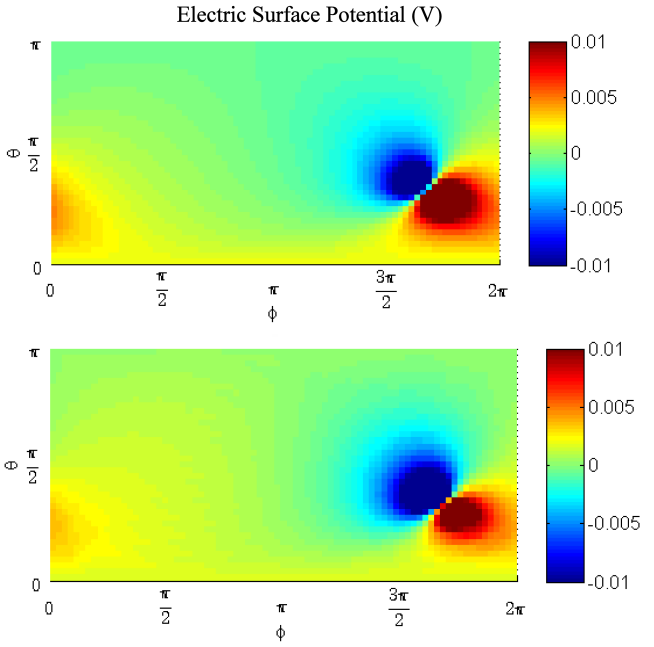

Fig. 3. Simulated EEG recordings originating from a spherical homogeneous conductor without (above) and including (below) deformations. The radius of the sphere model is $a = 0.071$ m whereas the conductivity equals $\sigma = 0.285$ S/m. The location of the dipole is $\mathbf{r}_0 = (0.06\,\mathrm{m}, \frac{5\pi}{16}, \frac{5\pi}{3})$ with moment $\mathbf{Q} = (10^{-5}, 10^{-5}, 10^{-5})$ Cm. This order of magnitude ensures that the measured potential is in mV per unit length [6].

In Fig. 3, the electric surface potentials generated by a dipole positioned exactly under the injury, are compared for the spherical homogeneous conductor without any deformation present (above) as well as the perturbed case (below). As expected, for active regions away from the distortion site potential recordings are not affected. However, for operating dipoles in the vicinity of the trauma (middle section of the right part of Fig. 3) modest differences for the entire measurements are observed. These differences intensify with the severity of the injury (shape and depth).

B. Deformation of the upper part of the head

The second example is concerned with the case where a large area, namely the upper part of the head, is deformed. This is an important case since: (a) it consist the main measurement site for EEG recordings and (b) human head shapes vary considerable among individuals.

The perturbed surface, depicted in Fig. 4, is constructed via (32) with parameters $(k,\ell,n,m) = (8,2,1,1)$ defined in the intervals $\theta \in [0, \frac{3\pi}{8}]$ and $\phi \in (0, 2\pi]$. The electric surface potentials for the unperturbed conductor (above) along with the perturbed case (below) are displayed in Fig. 5. The moment of the dipole source is considered the same as in the previous example sited at $\mathbf{r}_0 = (0.065\,\mathrm{m}, \frac{5\pi}{16}, \frac{3\pi}{2})$. Differences in the magnitude of the potential between 1 mV and 3 mV are observed affecting the entire spectrum of recordings. However, for deeper sources the influence of the shape of the (upper) head nearly vanishes.

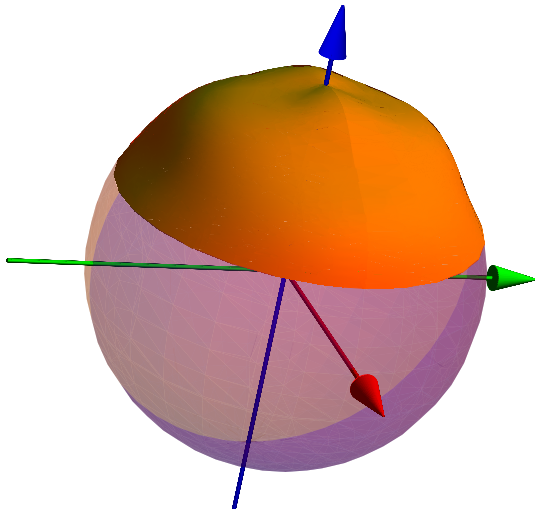

Fig. 4. A general deformation of the upper part of the human cranium. The red, green and blue arrows represent the x, y and z axis, respectively.

IV. CONCLUSIONS

We presented a first-order perturbation analysis in order to analyze the influence of geometric variations present on the conductors surface on the forward EEG problem. Such variations could represent the varying thickness of the skull, non-penetrating injuries associated with accidents or errors made in the process of building the head model. The results show that in the presence of geometric variations and for dipole sources near the brain surface, a slight divergences in the measured potentials up to 3 mV can be observed. These, although small differences, will have an impact on the inverse EEG problem, i.e. estimating the source position and strength.

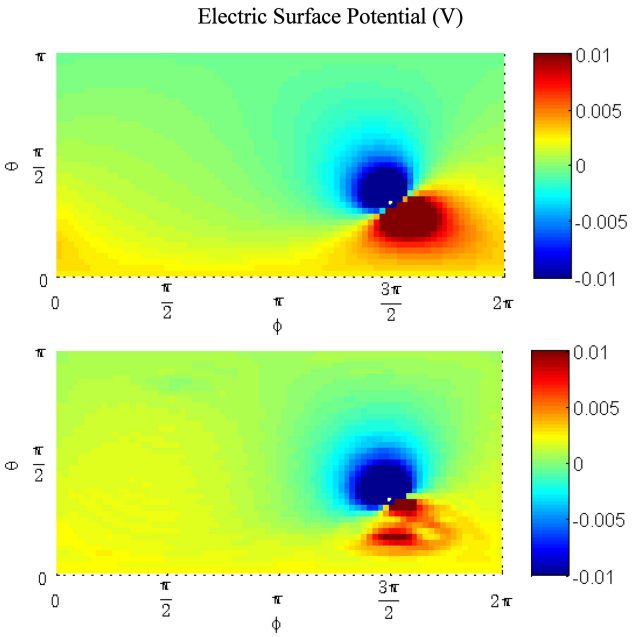

Fig. 5. The electric surface potential due to a dipole located at $\mathbf{r}_0 = (0.065\,\text{m}, \frac{5\pi}{16}, \frac{3\pi}{2})$ with moment $\mathbf{Q} = (10^{-5}, 10^{-5}, 10^{-5})$ Cm. The perturbation parameter is set to $\epsilon = 5 \times 10^{-3}$ m corresponding to a maximum-minimum departure from the unperturbed surface of $\pm 5 \times 10^{-3}$ m. The first graph displays the potential in the unperturbed case whereas the perturbed is shown in the second graph. The radius and conductivity take the same values given in Fig. 3.

V. ACKNOWLEDGMENTS

The authors gratefully acknowledge the contribution of the "ARISTEIA" Action of the "OPERATIONAL PROGRAMME EDUCATION AND LIFELONG LEARNING" co-funded by the European Social Fund (ESF) and National Resources.

REFERENCES

[1] B.N. Cuffin. Effects of local variations in skull and scalp thickness on EEG's and MEG's. IEEE Trans. Biomed. Eng. 40, pp. 42-48, 1993.

[2] N. Chauveau, X. Franceries, B. Doyon, B. Rigaud, J.P. Morucci and P. Celsis. Effects of skull thickness, anisotropy, and inhomogeneity on forward EEG/ERP computations using a spherical three-dimensional resistor mesh model. Hum Brain Mapp. 21(2), pp. 86-97, 2004.

[3] N. Ellenrieder, C.H. Muravchik and A. Nehorai. Effect of Geometric Head Model Perturbations on the EEG Inverse Problem. IEEE Trans. Biomed. Eng., 53(3), pp. 421-429, 2006.

[4] G. Dassios. Electric & Magnetic Activity of the Brain in Spherical and Ellipsoidal Geometry. In: Mathematical modeling in Biomedical Imaging I. H. Ammari (editor). Lecture Notes in Mathematics 1983. Springer, 2009.

[5] F.W.J. Olver, D.W. Lozier, R.F. Boisvert and C.W. Clark (Editors). NIST Handbook of Mathematical Functions. Cambridge University Press, 2010.

[6] H. Hallez *et al*. Review on solving the forward problem in EEG source analysis. Journal of NeuroEngineering and Rehabilitation, 4:46, 2007